Available online at www.sciencedirect.com
SCIENCE DIRECT®
International Journal of Heat and Mass Transfer 48 (2005) 1772–1784
International Journal of HEAT and MASS TRANSFER
www.elsevier.com/locate/ijhmt

Laminar mixed convection heat and mass transfer in vertical rectangular ducts with film evaporation and condensation

Chien-Chang Huang [a], Wei-Mon Yan [b,*], Jer-Huan Jang [c]

[a] Center for Environment Safety and Health Technology Development, Industrial Technology Research Institute, Chu Tung, Hsin Chu 310, Taiwan, ROC
[b] Department of Mechatronic Engineering, Huafan University, Shih Ting, Taipei 223, Taiwan, ROC
[c] Department of Mechanical Engineering, Northern Taiwan Institute of Science and Technology, Pei-To, Taipei 112, Taiwan, ROC

Received 13 May 2004; received in revised form 16 November 2004

Abstract

The investigation of mixed convection heat and mass transfer in vertical ducts with film evaporation and condensation has been numerically examined in detail. This work is primarily focused on the effect of film evaporation and condensation along the wetted wall with constant temperature and concentration on the heat and mass transfer in rectangular vertical ducts. The numerical results, including the distributions of dimensionless axial velocity, temperature and concentration distributions, Nusselt number as well as Sherwood number are presented for moist air mixture system with different wall temperatures and aspect ratios of the rectangular ducts. The results show that the latent heat transport with film evaporation and condensation augments tremendously the heat transfer rate. Better heat transfer enhancement related with film evaporation is found for a system with a higher wall temperature.

1. Introduction

Gas–liquid systems in which coupled heat and mass are transferred have been widely encountered in many practical applications. The processes such as film cooling, liquid film evaporator, cooling towers, cooling of microelectronic equipments, and the simultaneous diffusion of metabolic heat and perspiration in the control of human body temperature are some examples. Due to such widespread applications, heat and mass transfer of air stream with liquid film evaporation and condensation associated with latent heat transfer has received considerable attention.

The pioneer study concerning heat and mass transfer on condensation is by Minkowycz and Sparrow [1], which is an extension of Nusselt's original theory for a mixture of vapor and a non-condensable gas. The situation under their investigation is an isothermal vertical plate with steam as the condensing vapor and air as the non-condensable gas. In addition to the non-condensable gas, the analytical model includes interfacial resistance, superheating, free convection due to both temperature and concentration gradients, mass diffusion and thermal diffusion, and variable properties in both the liquid and the gas–vapor regions. It was found that a small bulk concentration of the non-condensable gas can have a decisive effect on the heat-transfer rate.

* Corresponding author. Tel.: +886 2 2663 2102; fax: +886 2 2663 1119.
E-mail address: wmyan@huafan.hfu.edu.tw (W.-M. Yan).

0017-9310/$ - see front matter © 2005 Elsevier Ltd. All rights reserved.
doi:10.1016/j.ijheatmasstransfer.2004.11.023

Nomenclature

A	cross-sectional area of vertical rectangular ducts (m)
a, b	width and height of vertical rectangular ducts, respectively (m)
c	dimensional species concentration
C	dimensionless species concentration, $(c - c_0)/(c_1 - c_0)$
c_p	specific heat (J kg^{-1} K^{-1})
D	mass diffusivity (m^2 s^{-1})
D_e	equivalent hydraulic diameter, $4A/S$ (m)
f	friction coefficient, $2\tau_w/(\rho_0 w_0^2)$
g	gravitational acceleration (m s^{-2})
Gr_T	heat transfer Grashof number, $g\beta(T_1 - T_0)D_e^3/\nu^2$
Gr_M	mass transfer Grashof number, $g\beta^*(c_1 - c_0)D_e^3/\nu^2$
h	average heat transfer coefficient (W m^{-2} K^{-1})
h_{fg}	latent heat of vaporization or condensation (J kg^{-1})
h_M	average mass transfer coefficient (m s^{-1})
k	thermal conductivity (W m^{-1} K^{-1})
M	molecular weight
n	dimensionless coordinate normal to a surface
Nu_l	local Nusselt number for latent heat transfer
Nu_s	local Nusselt number for sensible heat transfer
Nu_x	local Nusselt number ($=Nu_s + Nu_l$)
$\bar{p}$	cross-sectional mean pressure (kPa)
$\overline{P}$	dimensionless cross-sectional mean pressure
p'	perturbation term about mean pressure (kPa)
P'	dimensionless perturbation pressure
p_w	saturated water vapor pressure at the wetted wall
Pr	Prandtl number, ν/α
q_l	latent heat flux flowing into air stream (W m^{-2})
q_s	sensible heat flux flowing into air stream (W m^{-2})
q_x	interfacial total heat flux into air stream (W m^{-2})
Re	Reynolds number, $w_{o\ De}/\nu$
S	circumference of cross-section (m)
Sc	Schmidt number, ν/D
Sh	Sherwood number
T	temperature (K)
T_0	inlet temperature (K)
U, V, W	dimensionless velocity components in the X-, Y-, Z-directions, respectively
u, v, w	velocity components in the x-, y-, z-directions, respectively (m s^{-1})
V_e	dimensionless interfacial velocity of mixture in the y-direction
X, Y, Z	dimensionless rectangular coordinate, $X = x/D_e$, $Y = y/D_e$, $Z = z/(ReD_e)$
Z^*	dimensionless z-direction coordinate, $z/(PrReD_e) = Z/Pr$
x, y, z	rectangular coordinate system (m)

Greek symbols

α	thermal diffusivity (m^2 s^{-1})
β	coefficient of thermal expansion (1/K)
β^*	coefficient of concentration expansion, $M_a/M_v - 1$
γ	aspect ratio of a rectangular duct, a/b
ϕ	relative humidity of moist air in the ambient
ν	kinematic viscosity (m^2 s^{-1})
ξ	dimensionless vorticity in the axial direction, defined in Eq. (8)
ρ	density (kg m^{-3})
θ	dimensionless temperature, $(T - T_0)/(T_1 - T_0)$

Superscript

–	mean quantity

Subscripts

1	condition at porous wetted wall 1; i.e., at $y = 0$
2	condition at porous wetted wall 2; i.e., at $y = b$
a	of air
b	bulk fluid quantity
f	fully-developed quantity before thermal entrance
M	caused by mass
0	condition at inlet
T	caused by temperature
v	of water vapor
w	value at wall

The case of evaporation of water by superheated steam has also received much attention in many theoretical and experimental studies. Wenzel and White [2] and Chu et al. [3] were the first to show experimentally that more evaporation occurs in superheated vapor than in air. Chow and Chung [4,5] presented the first numerical

studies of the evaporation of water into dry air and superheated steam for a laminar and turbulent forced convection over a flat plate. Because of the complexity of couplings between the momentum, heat and mass transfer in the flow, they focused on heat and mass transfer in a gas stream by assuming the liquid film to be extremely thin and found that mass transfer associated with the film evaporation has a pronounced impact on the heat transfer. Recently, Debbissi et al. [6,7] numerically investigated the coupled heat and mass transfer by natural or mixed convection during water evaporation into air and humid air in a vertical heated channel. They discovered that the evaporative cooling changes the profiles of velocity and temperature considerably especially at the exit of the channel. Hammou et al. [8] have studied the effects of simultaneous heat and mass transfer on downward laminar flow of humid air in a vertical channel with isothermal wet walls numerically using an elliptical formulation. They found that the effects of the buoyancy forces on the hydrodynamic field are very important while their influence on the average air temperature and average mass fraction is small. Even though sensible heat is always transferred from the air to the walls, the latter must be heated when evaporation is important.

Yan and co-workers [9–13] and Fedorov et al. [14] investigated the influences of wetted wall on laminar or turbulent mixed convection heat and mass transfer in vertical channels. The results showed that the effects of the evaporation of water vapor on the heat transfer are rather substantial. As for the studies on the mixed convection heat and mass transfer in rectangular ducts, Lin et al. [15] presented a pioneer study. They considered the combined buoyancy effects resulting from the thermal and mass buoyancies on the forced convection in a horizontal duct.

Knowing from the paper review cited above, despite its practical importance, the mixed convection heat and mass transfer in vertical rectangular ducts with film evaporation and condensation has not been well evaluated. This motivates the present study. In this work, an attempt is made to analyze the heat and mass transfer in vertical rectangular ducts with latent heat transport at the two walls of constant temperatures. The main objective of this study is to extend the understanding of water condensation at the constant wall and evaporation into the moist air in a laminar mixed convection flow.

2. Analysis

Consider a steady three-dimensional laminar uniform flow of moist air mixture in the entrance region of a vertical rectangular duct, as schematically shown in Fig. 1. The width and height of the rectangular ducts are a and b, respectively. The rectangular duct has insulated solid

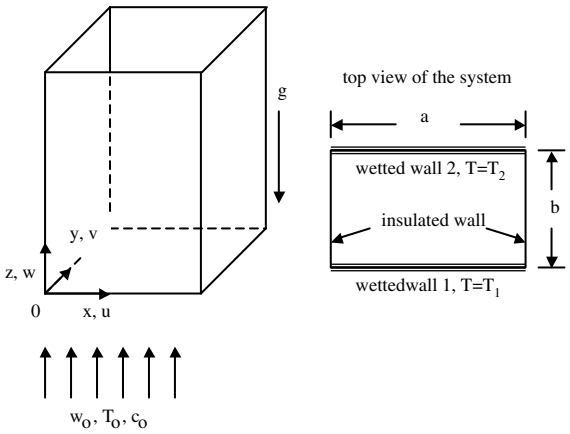

Fig. 1. Schematic diagram of the physical system.

walls on both sides in the x-direction. The porous duct walls in the y-direction are wetted by the thin liquid films and maintained at constant temperatures, T_1 for wetted wall 1 and T_2 for wetted wall 2, respectively. The u, v and w are the velocity components in the x-, y- and z-directions, respectively. The air–water mixture entering into the duct has a uniform axial velocity w_0, temperature T_0, concentration c_0, and relative humidity ϕ.

The thermo-physical properties of the mixture are assumed to be constant and evaluated by the one-third rule [4,16] except for density variation in the buoyancy term in the z-momentum equation. The complete details on the evaluation of the properties of air, steam and their mixture are available in Refs. [17–19]. In this study, the Boussinesq approximation is used to characterize the buoyancy effect [20]. In order to simplify the problem, the liquid films on the wetted porous walls are assumed to be extremely thin so that they can be treated as boundary conditions. Actually, the liquid films on the wetted walls are of finite thickness and move downwards due to gravity effect and interact with the moist air mixture. However, this would complicate the present problem. It is found that the assumption of extremely thin film thickness is reasonable as the film thickness is relatively thin [21]. In addition, an order of magnitude analysis is employed which deduces the governing equations by neglecting the axial diffusion of momentum, heat and mass [22–24]. This is justified as the Peclect number is high enough, e.g., $Pe > 100$ [25]. In this analysis, the species diffusion processes exist in a very low concentration level, resulting that the diffusion-thermo (Dufour) and thermo-diffusion (Soret) effects can be neglected, as well as negligible interfacial velocities from species diffusion at the surface.

The governing equations are those of conservation of mass, momentum, energy and concentration. By introducing the following dimensionless variables:

$$D_e=\frac{4A}{S},\quad X=\frac{x}{D_e},\quad Y=\frac{y}{D_e},\quad Z=\frac{z}{ReD_e},$$
$$U=\frac{uD_e}{v},\quad V=\frac{vD_e}{v},\quad W=\frac{w}{w_0},\quad \overline{P}=\frac{\overline{p}}{\rho_0 w_0^2},$$
$$P'=\frac{p'}{\rho_0 v^2/D_e^2},\quad \theta=\frac{T-T_0}{T_1-T_0},\quad c=\frac{c-c_0}{c_1-c_0},$$
$$Z^*=\frac{Z}{Pr},\quad \gamma=\frac{a}{b},\quad Re=\frac{w_0D_e}{v},\quad Pr=\frac{v}{\alpha},\quad Sc=\frac{v}{D},$$
$$Gr_T=\frac{g\beta_T(T_1-T_0)D_e^3}{v^2},\quad Gr_M=\frac{g\beta^*(c_1-c_0)D_e^3}{v^2} \tag{1}$$

and with the assumptions made earlier, the non-dimensional governing equations can be formulated as follows:

Continuity equation

$$\frac{\partial U}{\partial X}+\frac{\partial V}{\partial Y}+\frac{\partial W}{\partial Z}=0 \tag{2}$$

Momentum equations

$$U\frac{\partial U}{\partial X}+V\frac{\partial U}{\partial Y}+W\frac{\partial U}{\partial Z}=-\frac{\partial P'}{\partial X}+\frac{\partial^2 U}{\partial X^2}+\frac{\partial^2 U}{\partial Y^2} \tag{3}$$

$$U\frac{\partial V}{\partial X}+V\frac{\partial V}{\partial Y}+W\frac{\partial V}{\partial Z}=-\frac{\partial P'}{\partial Y}+\frac{\partial^2 V}{\partial X^2}+\frac{\partial^2 V}{\partial Y^2} \tag{4}$$

$$U\frac{\partial W}{\partial X}+V\frac{\partial W}{\partial Y}+W\frac{\partial W}{\partial Z}=-\frac{\partial \overline{P}}{\partial Z}+\frac{\partial^2 W}{\partial X^2}+\frac{\partial^2 W}{\partial Y^2}+\frac{1}{Re}(Gr_T\theta+Gr_M C) \tag{5}$$

Energy equation

$$U\frac{\partial \theta}{\partial X}+V\frac{\partial \theta}{\partial Y}+W\frac{\partial \theta}{\partial Z}=\frac{1}{Pr}\left(\frac{\partial^2\theta}{\partial X^2}+\frac{\partial^2\theta}{\partial Y^2}\right) \tag{6}$$

Concentration equation

$$U\frac{\partial C}{\partial X}+V\frac{\partial C}{\partial Y}+W\frac{\partial C}{\partial Z}=\frac{1}{Sc}\left(\frac{\partial^2 C}{\partial X^2}+\frac{\partial^2 C}{\partial Y^2}\right) \tag{7}$$

It should be noted that the flow is assumed to be parabolic [22–24] and in the z-direction momentum equation a space-averaged pressure $\overline{P}$ is imposed to prevail at each cross-section, permitting a decoupling of the pressure in the cross-sectional momentum equation by making the usual parabolic assumption [26]. The dynamic pressure can be presented as the sum of a cross-sectional mean pressure $\overline{P}(Z)$, which derives the main flow and a perturbed pressure about the mean, $P'(X, Y)$, which derives the cross-stream flow. The 'Pressure uncoupling' follows the parabolic-flow practice and, together with the neglect of axial diffusion momentum, heat and concentration by an order of analysis, permits a marching-integration calculation procedure. The vorticity–velocity method developed by Ramakrishna et al. [20] is employed in the study. Introducing the axial vorticity, ξ:

$$\xi=\frac{\partial U}{\partial Y}-\frac{\partial V}{\partial X} \tag{8}$$

the axial vorticity equation can be derived from Eqs. (3) and (4),

$$U\frac{\partial \xi}{\partial X}+V\frac{\partial \xi}{\partial Y}+W\frac{\partial \xi}{\partial Z}+\xi\left(\frac{\partial U}{\partial X}+\frac{\partial V}{\partial Y}\right)+\left(\frac{\partial W}{\partial Y}\cdot\frac{\partial U}{\partial Z}-\frac{\partial W}{\partial X}\cdot\frac{\partial V}{\partial Z}\right)=\frac{\partial^2\xi}{\partial X^2}+\frac{\partial^2\xi}{\partial Y^2} \tag{9}$$

The equations of the transverse velocity components (U, V) can be formulated from the continuity, and the definition of axial vorticity as

$$\frac{\partial^2 U}{\partial X^2}+\frac{\partial^2 U}{\partial Y^2}=\frac{\partial \xi}{\partial Y}-\frac{\partial^2 W}{\partial X\partial Z} \tag{10}$$

$$\frac{\partial^2 V}{\partial X^2}+\frac{\partial^2 V}{\partial Y^2}=-\frac{\partial \xi}{\partial X}-\frac{\partial^2 W}{\partial Y\partial Z} \tag{11}$$

The corresponding boundary conditions are

Entrance ($Z=0$)

$$W=1;\quad U=V=\xi=\theta=C=0 \tag{12a}$$

Midplane [$X=(1+\gamma)/4$]

$$\frac{\partial W}{\partial X}=U=\frac{\partial V}{\partial X}=\frac{\partial \theta}{\partial X}=\frac{\partial C}{\partial X}=0 \tag{12b}$$

Duct walls

$$U=V=W=0;\quad \frac{\partial\theta}{\partial X}=\frac{\partial C}{\partial X}=0\quad \text{at } X=0 \tag{12c}$$

$$U=W=0;\quad V=V_{e1};\quad C=1;\quad \theta=1\quad \text{at } Y=0 \tag{12d}$$

$$U=W=0;\quad V=V_{e2};\quad C=C_2;\quad \theta=\theta_2\quad \text{at } Y=(1+\gamma)/2\gamma \tag{12e}$$

Since the air–water interface is semi-permeable (the solubility of air in water is negligibly small and air velocity in the direction normal to the porous wetted wall is zero with no-slip condition at the interface), the evaporating or condensing velocities of the mixture on the wetted walls are evaluated by Burmeister [27],

$$V_{ei}=-\frac{(c_1-c_0)}{Sc(1-c_i)}\frac{\partial C}{\partial Y},\quad i=1,2 \tag{13}$$

where the subscript $i=1$ represents the condition on the wetted wall 1 [$Y=0$], while $i=2$ indicates the condition on wetted wall 2 [$Y=(1+\gamma)/2\gamma$]. According to Dalton's law and the state equation of ideal gas mixture, the interfacial mass fraction of water vapor can be calculated by

$$c_i=\frac{p_{wi}M_v}{p_{wi}M_v+(p-p_{wi})M_a},\quad i=1,2 \tag{14}$$

where p_w is the saturated water vapor pressure on the wetted walls. One constraint to be satisfied is that the

overall mass flow rate at every axial location must be balanced in the duct flow:

$$\int_0^{\frac{1+\gamma}{2\gamma}}\int_0^{\frac{1+\gamma}{4}} W\,\mathrm{d}X\,\mathrm{d}Y = \frac{(1+\gamma)^2}{8\gamma} + \int_0^{Z}\int_0^{\frac{1+\gamma}{4}} (V_{e1}-V_{e2})\,\mathrm{d}X\,\mathrm{d}Z \tag{15}$$

This equation is utilized to obtain the axial pressure gradient in Eq. (5).

After obtaining the developing velocity, temperature and concentration fields along the axial direction of the vertical rectangular duct, the local friction coefficient, Nusselt and Sherwood numbers are major parameters of practical interest for the study of convection heat and mass transfer. Following the usual definitions, the expression for the product of the peripherally averaged friction factor and Reynolds number can be expressed as

$$fRe = -2\overline{\left.\frac{\partial W}{\partial n}\right|}_{\text{wall}} \tag{16}$$

where the overbar stands for the average around the perimeters.

Energy transport between the wetted wall 1 and the fluid in the duct in the presence of mass transfer depends on two factors: (1) the fluid temperature gradient at the wetted wall 1, resulting in a sensible heat transfer; (2) the rate of mass transfer, resulting in a latent heat transfer. Therefore, the total heat flux from the wetted wall 1 can be expressed as

$$q_{x1} = q_{s1} + q_{l1} = -k\left.\frac{\partial T}{\partial y}\right|_1 - \frac{\rho D h_{fg}}{1-c_1}\cdot\left.\frac{\partial c}{\partial y}\right|_1 \tag{17}$$

where q_x, q_s and q_l denote the interfacial heat flux, sensible heat flux and latent heat flux, respectively. In the same manner, the total heat flux from the wetted wall 2 can be formulated as follows:

$$q_{x2} = q_{s2} + q_{l2} = k\left.\frac{\partial T}{\partial y}\right|_2 + \frac{\rho D h_{fg}}{1-c_2}\cdot\left.\frac{\partial c}{\partial y}\right|_2 \tag{18}$$

The locally averaged Nusselt numbers along the wetted surfaces are defined as

$$Nu_{xi} = \frac{h_i D_e}{k} = \frac{q_{xi} D_e}{k(T_1 - T_b)}, \quad i = 1,2 \tag{19}$$

and can then be written as

$$Nu_{xi} = Nu_{si} + Nu_{li}, \quad i = 1,2 \tag{20}$$

where Nu_s and Nu_l are the local Nusselt numbers for sensible and latent heat transfer, respectively, and they are defined as the following:

$$Nu_{si} = \frac{1}{1-\theta_b}\left.\frac{\overline{\partial\theta}}{\partial n}\right|_i, \quad i = 1,2 \tag{21a}$$

$$Nu_{li} = S_i^*\frac{1}{1-\theta_b}\cdot\frac{1}{1-c_i}\cdot\left.\frac{\overline{\partial C}}{\partial n}\right|_i, \quad i = 1,2 \tag{21b}$$

where S^* indicates the importance of the energy transport through species diffusion relative to that through heat conduction

$$S_i^* = \frac{\rho D h_{fgi}(c_1 - c_0)}{k(T_1 - T_0)}, \quad i = 1,2 \tag{22}$$

Similarly, the Sherwood numbers on the wetted walls can be formulated as follows:

$$Sh_i = \frac{1}{1-C_b}\left.\frac{\overline{\partial C}}{\partial n}\right|_i, \quad i = 1,2 \tag{23}$$

The bulk fluid temperature θ_b and bulk fluid concentration C_b are defined as

$$\theta_b = \frac{\int_0^{\frac{1+\gamma}{2\gamma}}\int_0^{\frac{1+\gamma}{4}}\theta\cdot W\,\mathrm{d}X\,\mathrm{d}Y}{\int_0^{\frac{1+\gamma}{2\gamma}}\int_0^{\frac{1+\gamma}{4}} W\,\mathrm{d}X\,\mathrm{d}Y}, \quad C_b = \frac{\int_0^{\frac{1+\gamma}{2\gamma}}\int_0^{\frac{1+\gamma}{4}} C\cdot W\,\mathrm{d}X\,\mathrm{d}Y}{\int_0^{\frac{1+\gamma}{2\gamma}}\int_0^{\frac{1+\gamma}{4}} W\,\mathrm{d}X\,\mathrm{d}Y} \tag{24}$$

3. Numerical approach

In present work, the governing equations are solved by the vorticity–velocity method for three-dimensional parabolic flow [20] for the velocities, temperature and concentration. The detailed numerical method and solution procedure are available in Ref. [28] and are not presented here. In the present study, the uniform cross-sectional meshes were chosen, while the z-direction grid spacing was non-uniform with grid lines being more closely packed near the entrance. In this work, the grid points used in the x- and y-directions are selected to be 51 (M) and 51 (N), respectively. The axial step size ΔZ^* was varied from 2×10^{-6} near the duct entrance to about 1×10^{-3} near the fully-developed region. To examine the grid size effects, Table 2 presents the local Nusselt number on wetted wall 1 for case 2 for various grid arrangements. It is clear that the deviations in the local Nusselt number are less than 2% between the results of the axial step size ΔZ^* of (2×10^{-6}–1×10^{-3}) and (5×10^{-7}–1×10^{-3}). In addition, various grid arrangements of cross-sectional grid points ($M\times N$) are tested. It is found in Table 2 that the deviations in the local Nusselt number between the cross-sectional grid points ($M\times N$) of 51×51 and 71×71 are within 2%. Furthermore, as a partial verification of the computation procedure, results were initially obtained for mixed convection heat transfer in horizontal rectangular duct without film evaporation. The results are compared with those of Abou-Ellail and Morcos [29]. The Nusselt numbers were found to agree within 3%. Through these program tests, the solution method and the formulation adopted are appropriate for the present study.

Table 1
Values of the major parameters

Case	T_1 (°C)	T_2 (°C)	ϕ (%)	Re	Gr_T	Gr_M	Pr	Sc	γ
1	30	30	50	2000	37,156	12,765	0.706	0.594	1
2	50	30	50	2000	97,196	41,712	0.701	0.588	1
3	70	30	50	2000	145,156	108,402	0.704	0.575	1
4	50	30	10	2000	97,098	45,002	0.701	0.588	1
5	50	30	90	2000	97,295	38,393	0.701	0.587	1
6	50	30	50	1000	97,196	41,712	0.701	0.588	1

Table 2
Effects of grid size on local Nusselt number on wetted wall 1 for case 2

$M \times N(\Delta Z^*)$	Z^*					
	0.001	0.005	0.01	0.05	0.1	0.3
$51 \times 51(2 \times 10^{-6}$–$1 \times 10^{-3})$	89.15	45.42	34.32	18.40	13.40	6.98
$71 \times 71(2 \times 10^{-6}$–$1 \times 10^{-3})$	89.24	45.33	34.21	18.31	13.39	6.92
$31 \times 31(2 \times 10^{-6}$–$1 \times 10^{-3})$	93.93	45.95	34.58	18.52	13.48	7.11
$51 \times 51(1 \times 10^{-6}$–$1 \times 10^{-3})$	88.96	45.2	34.42	18.43	13.36	6.97
$51 \times 51(5 \times 10^{-7}$–$1 \times 10^{-3})$	88.96	45.43	34.41	18.41	13.36	6.97

4. Results and discussion

For the present study, calculations are specifically performed for moist air flowing in vertical rectangular ducts. Other mixtures can also be determined similarly. According to the previous analysis, mixed convection heat and mass transfer depends on Re, Pr, Sc, Gr_T, Gr_M, γ and also on T_1. It should be recognized that not all values of the non-dimensional parameters could be arbitrarily assigned. Actually, they are interdependent for a given mixture under certain specific conditions. Instead of physical parameters—the temperature of wetted wall 1, the relative humidity of the ambient moist air, the inlet Reynolds number, and the aspect ratio—are picked as the independent variables.

In this study, the incoming air mixture at the inlet is fixed at 20 °C and 1 atm, the relative humidity is chosen to be 10%, 50% or 90%, the wetted wall 1 is kept at a uniform temperature being 30, 50 or 70 °C, the wetted wall 2 is maintained at a constant temperature of 30 °C, and the through-flow Reynolds number at the inlet is assigned to 1000 or 2000. Based on the above specific conditions, all the non-dimensional parameters can then be calculated. Results are obtained for six cases presented in Table 1, where case 2 is the typical case for comparison and the aspect ratio for each case is 1. Additionally, in order to investigate the geometry effects on the mixed convection heat and mass transfer, the aspect ratios are chosen to be 1, 2 and 5. Numerical solutions were obtained for the distributions of axial velocity, temperature and concentration profiles, the local friction coefficient, Nusselt and Sherwood numbers.

4.1. Development of dimensionless axial velocity, temperature and concentration

The development of axial velocity, temperature and concentration profiles are of engineering interest and useful in clarifying the heat and mass transfer mechanism. Fig. 2 shows axial velocity contours in the vertical duct cross-section at $Z^* = 0.001$, 0.04, 0.1 and 0.3 for cases 2, 3 and 6. Near the entrance of the duct, the axial velocities are fairly uniform because of developing flow. In this region, buoyancy effects are still weak and the iso-velocity distributions are seen to be nearly symmetric. As the flow goes downstream, the velocity in the core region is accelerated due to the entrance effect. It is clearly observed that the velocity profiles develop gradually from uniform distributions at the inlet to the parabolic ones in the fully-developed region. As the flow moves downstream, the mass flow rate is larger for the system with a higher wetted wall temperature T_1 in association with higher film evaporation rate along the wetted walls, and the peak axial velocity moves towards the wetted wall 1 (i.e., $Y = 0$). The asymmetric buoyancy forces of thermal and concentration diffusion cause the distortion of velocity profiles. This is readily explained by the fact that the combined buoyancy forces are stronger near the wetted wall 1. A comparison of cases 2 and 6 in Fig. 2 indicates that a significant distortion of axial velocity is noted for the case 6. This can be made plausible by noting the fact that the mixed convection effects are stronger for a system with a lower Reynolds number when the system is subjected to the same buoyancy forces.

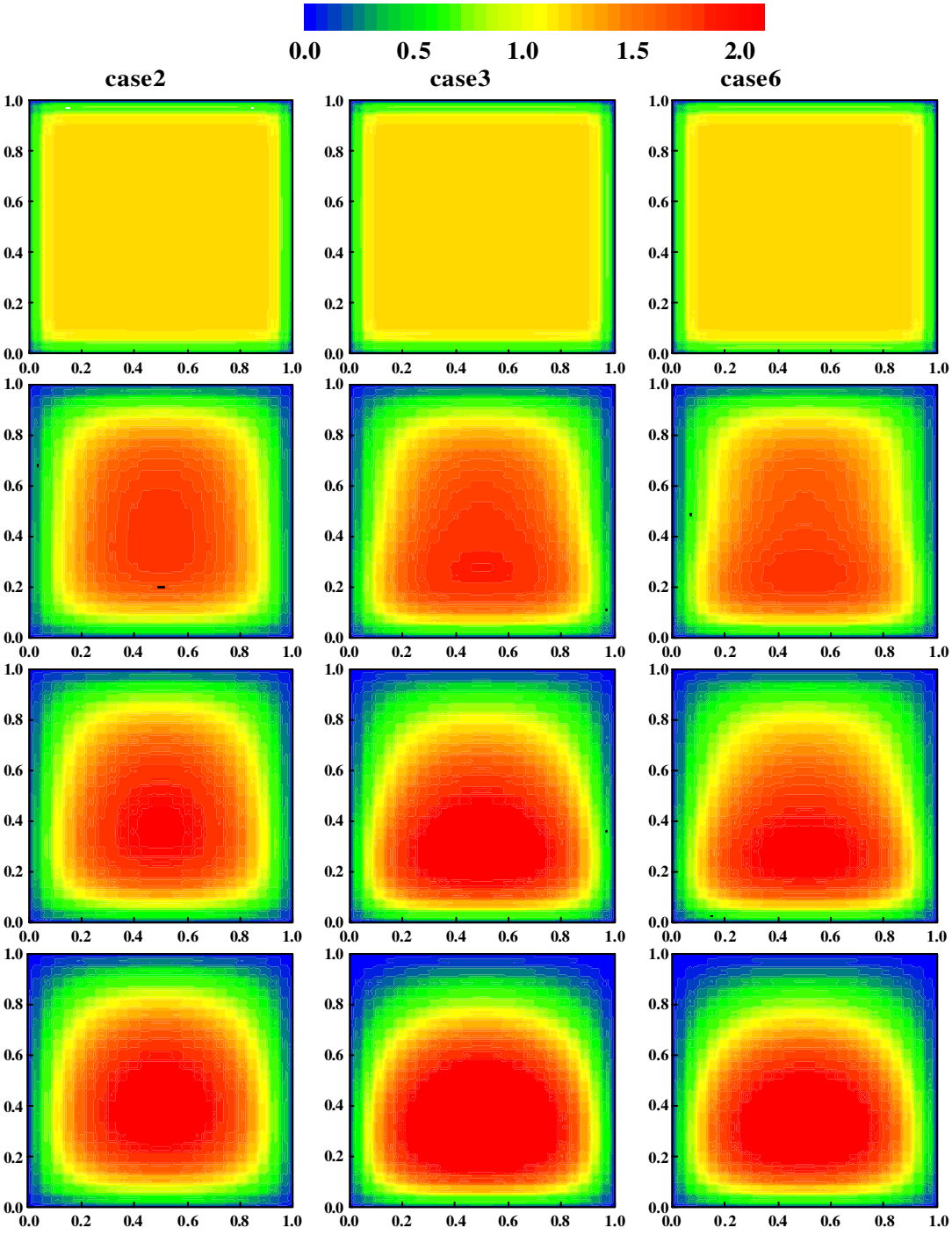

Fig. 2. The iso-velocity contours at certain locations for cases 2, 3 and 6 for $\gamma = 1$.

The contours of the isotherm and iso-concentration at different axial locations are shown in Figs. 3 and 4, respectively. The isotherm and iso-concentration contours develop in a similar pattern because the concentration equation and energy equation are similar. The only difference between them is *Pr* for energy equation and *Sc* for concentration equation. A careful inspection of Figs. 3 and 4 discloses that the concentration boundary layers

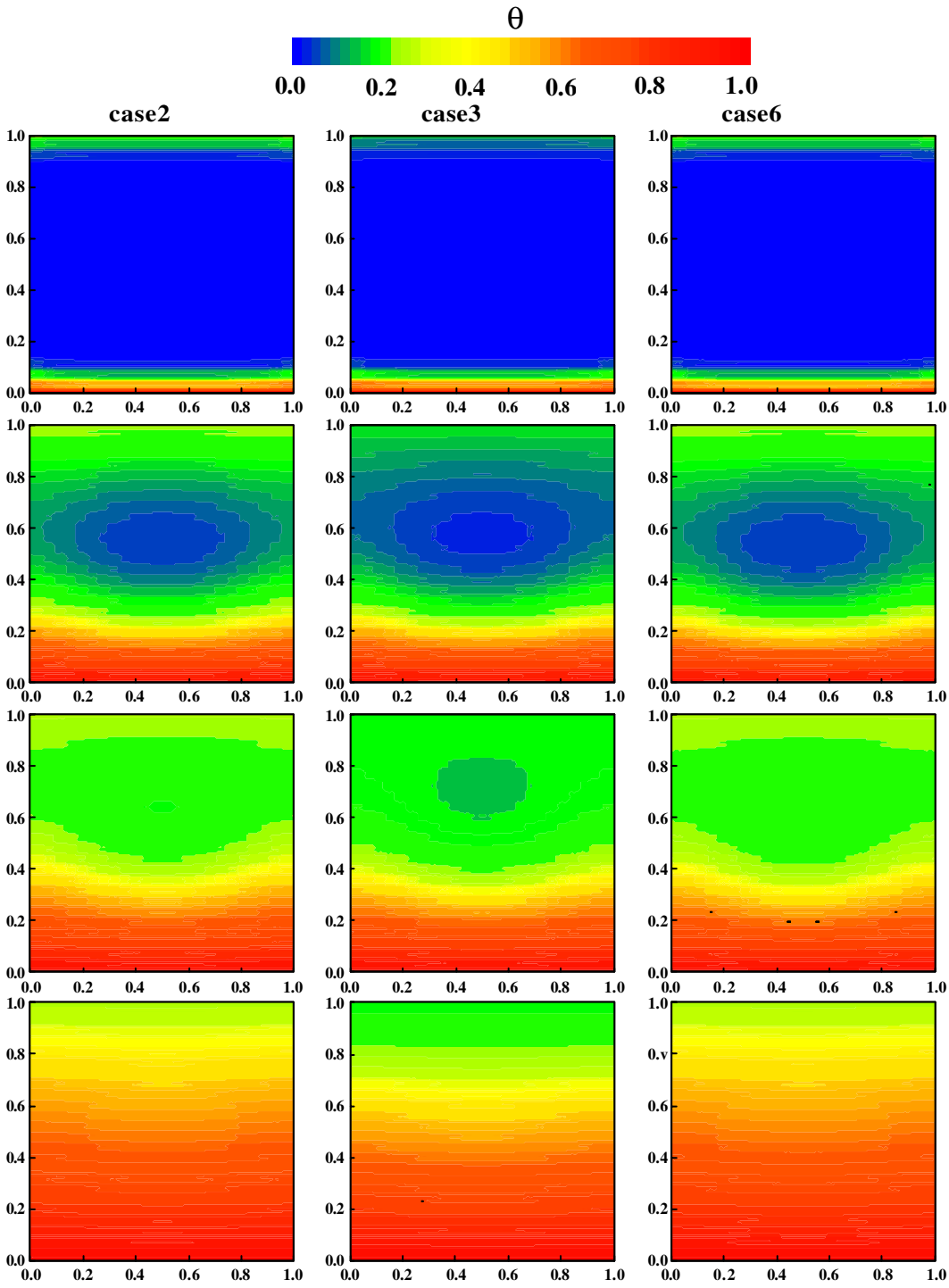

Fig. 3. The isotherm contours at certain locations for cases 2, 3 and 6 for $\gamma = 1$.

develop more rapidly than the thermal boundary layers do. This is simply due to the fact that *Pr* is slightly larger than *Sc* in the flow (see Table 1). Comparison of cases 2 and 3 in Fig. 4 indicates that the concentration of water vapor in the flow is small in the initial portion of the duct, but as the flow goes downstream, the

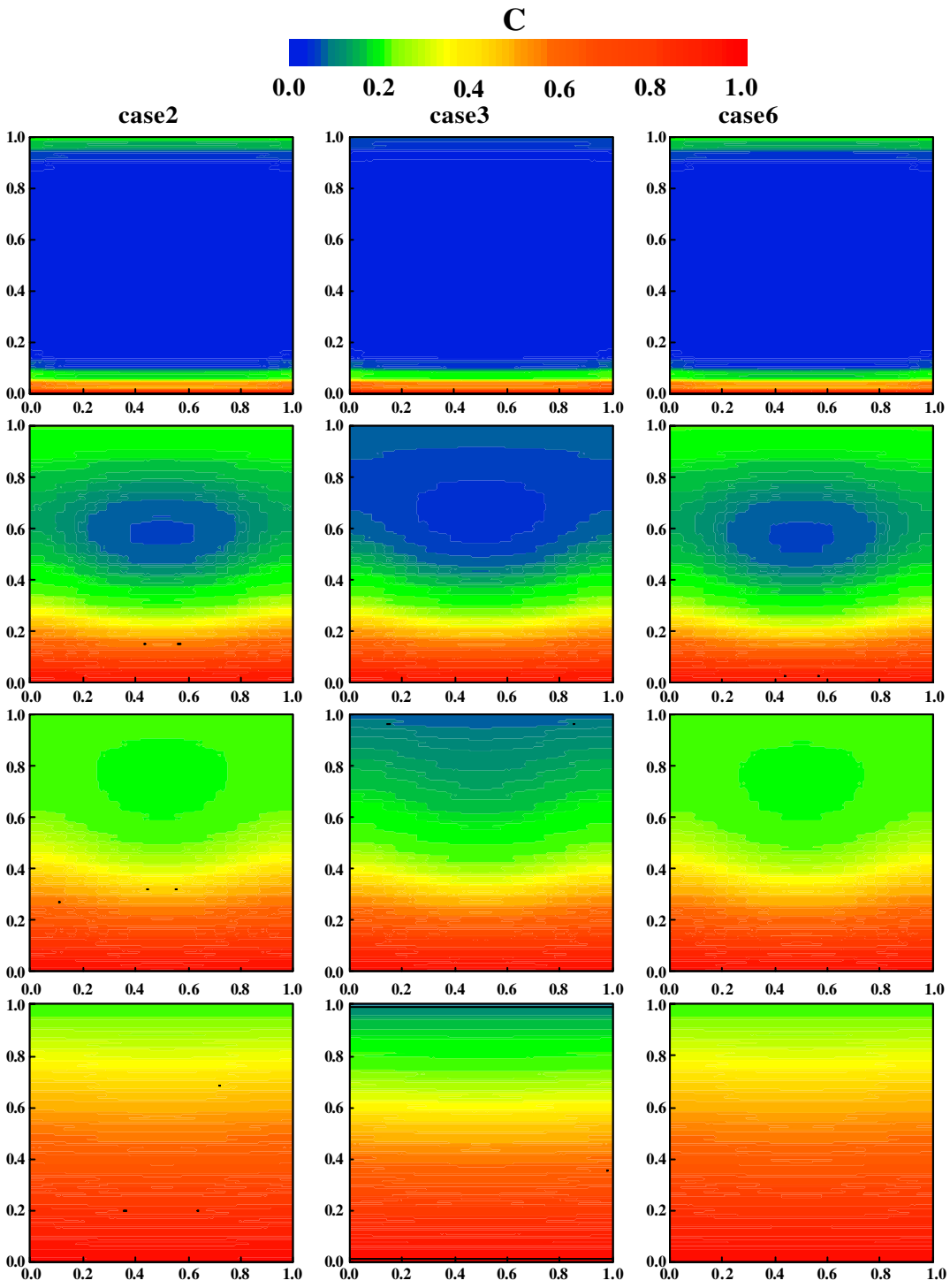

Fig. 4. The iso-concentration contours at certain locations for cases 2, 3 and 6 for $\gamma = 1$.

concentration of water vapor gradually increases because of the liquid film vaporization from the wetted walls. Therefore, the concentration level of water vapor near the wetted wall 2 could be higher than that on the wetted wall 2 beyond a certain axial location. This implies that the water vapor in the flow will condense on

the wetted wall 2 after this location. Therefore, the film evaporation takes place on the wetted wall 2 near the entrance region, but the condensation of water vapor in the air mixture may occurs in the downstream region.

4.2. Axial distributions of friction coefficient, Nusselt and Sherwood numbers

4.2.1. Effects of aspect ratio γ

Geometry effect is one of the importance parameters on the convection heat and mass transfer. Figs. 5–7 show the effects of the aspect ratio γ on local friction coefficient, Nusselt and Sherwood numbers for $\gamma = 1$, 2 and 5. It is clear in Fig. 5 that the local friction coefficient is high in the entrance region due to the entrance effect. But as the flow develops along the axial location, the friction coefficient decreases and approaches a fully developed value, depending on the aspect ratio. It is also clearly seen in Fig. 5 that the friction coefficient increases with an increase in the aspect ratio. It means that when the wetted wall is wider, the friction coefficient is higher with the same Reynolds number.

Fig. 6 presents the influence of aspect ratio γ on the local heat transfer rates on the wetted walls 1 and 2. It seems that the effects of the aspect ratios on the local Nusselt number on the wetted wall 1 are not significant. However, as the aspect ratio increases, the local Nusselt number on the wetted wall 2 decreases for a fixed axial location, as shown in Fig. 6(b). This is because that the wetted wall 2 has a larger area, which in turn causes a larger condensing water vapor. In Fig. 7, a similar behavior is noted for the local Sherwood number. This is owing to the fact that the *Pr* and *Sc* are of order 1 (please see Table 1).

4.2.2. Effects of wetted wall temperature T_1 and Reynolds number Re

Fig. 8 presents the effects of wetted wall temperature T_1 and Reynolds number *Re* on the local friction coefficient distributions. A higher T_1 shows a larger friction

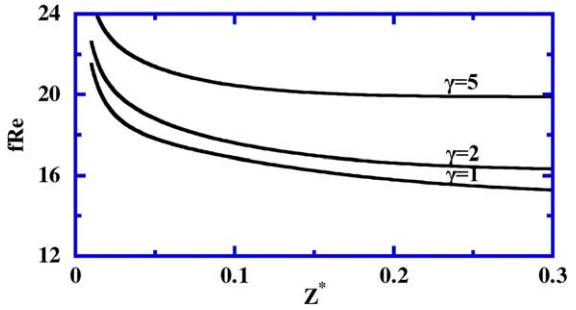

Fig. 5. Effects of aspect ratios γ on local friction coefficient distributions for case 2.

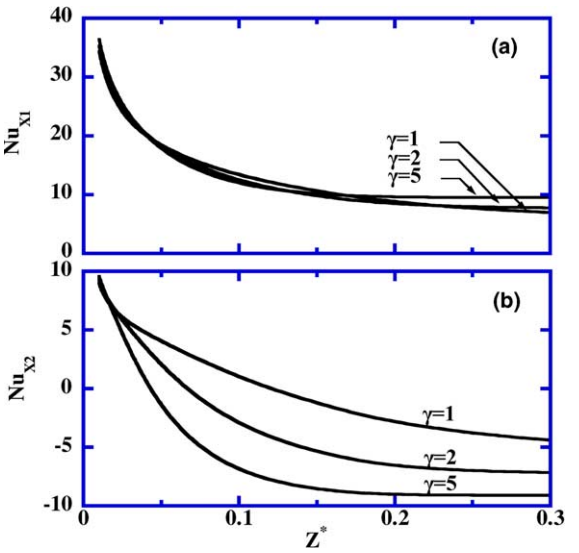

Fig. 6. Effects of aspect ratios γ on local Nusselt number distributions for case 2 on the (a) wetted 1 and (b) wetted wall 2.

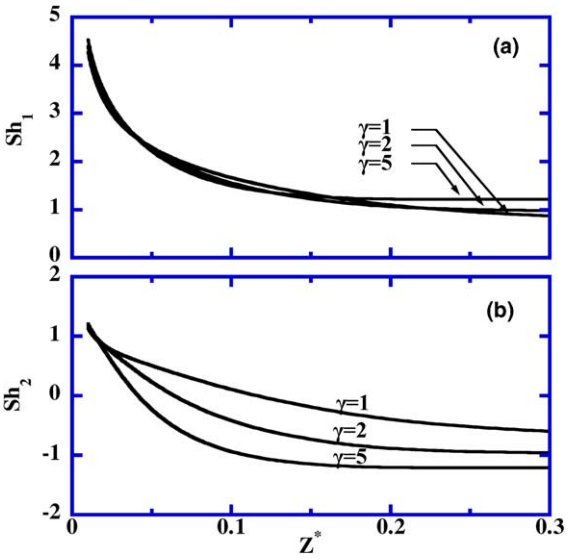

Fig. 7. Effects of aspect ratios γ on local Sherwood number distributions case 2 on the (a) wetted wall 1 and (b) wetted wall 2.

coefficient. This can be explained by the fact that a higher T_1 would cause a larger combined buoyancy forces, which in turn, lead to a higher friction coefficient. By comparing cases 2 and 6, it is found that a decrease in *Re* would raise the friction coefficient in flow, especially in the developing flow region where combined buoyancy forces of thermal and mass diffusion are more effective with less inertia force.

To study the relative contributions of heat transfer through latent and sensible heat exchanges in the flow,

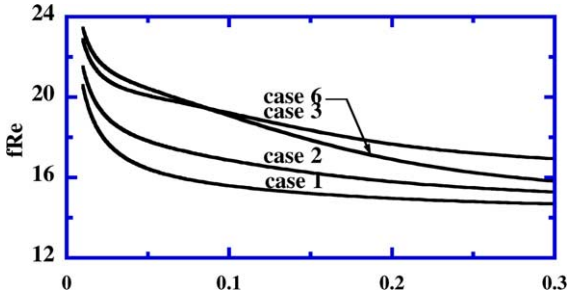

Fig. 8. Effects of wetted wall temperature T_1 on local friction coefficient distributions for $\gamma = 1$.

both latent and sensible heat transfer Nusselt numbers are illustrated in Figs. 9 and 10. An overall inspection on Fig. 9 reveals that a larger Nu_s is noted for a higher T_1 due to a greater buoyancy forces. And, the latent heat transport associated with the film evaporation is much more effective than that due to sensible heat transport connected to the temperature difference. Furthermore, the flow with higher T_1 shows a larger Nu_l. This is brought about by the larger latent heat transport in associated with the larger liquid film evaporation for a high T_1. The influence of Re on the local heat transfer is also included in Fig. 9. It shows that Re has no influence on the heat and mass transfer.

In Fig. 10, it is observed that the local Nusselt numbers along the wetted wall 2 decreases as T_1 increases by comparing cases 1, 2 and 3. Near the entrance, both Nu_s and Nu_l are positive. It means that the heat is transferred from the wetted wall 2 to the flow because the wetted wall temperature T_2 is higher than the flow. Bur after certain axial location, the condensation of water vapor takes place along the wetted wall 2, which in turn, causes negative values of Nu_s and Nu_l for cases 2 and 3.

Fig. 11 shows the effects of T_1 and Re on the local mass transfer along the wetted walls. In Fig. 11, the distributions of Sherwood numbers resemble those of Nu_s in Figs. 9 and 10. This is because the Pr and Sc are of the same order of magnitude. It is clear that the local Sherwood number along wetted wall 1 increases as T_1

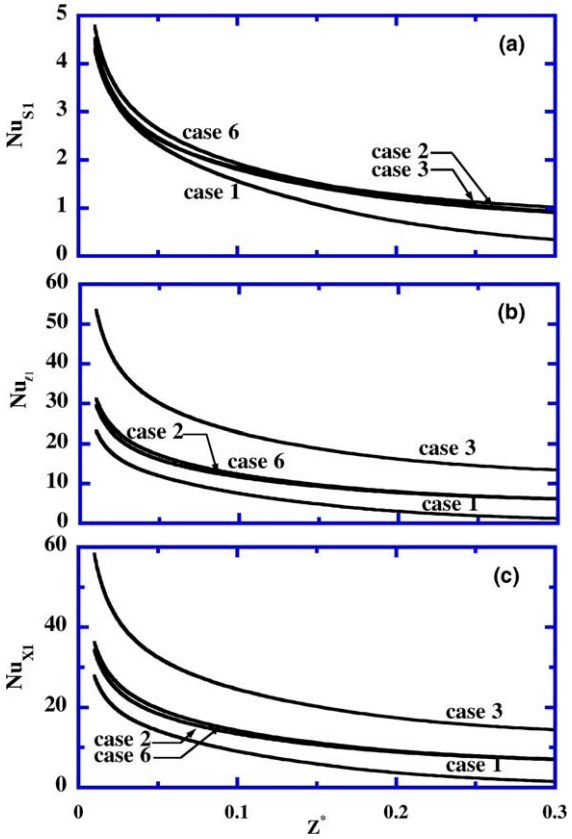

Fig. 9. Effects of wetted wall temperature T_1 on local Nusselt number distributions on the wetted wall 1 for $\gamma = 1$: (a) sensible heat Nusselt number; (b) latent heat Nusselt number; (c) interfacial Nusselt number.

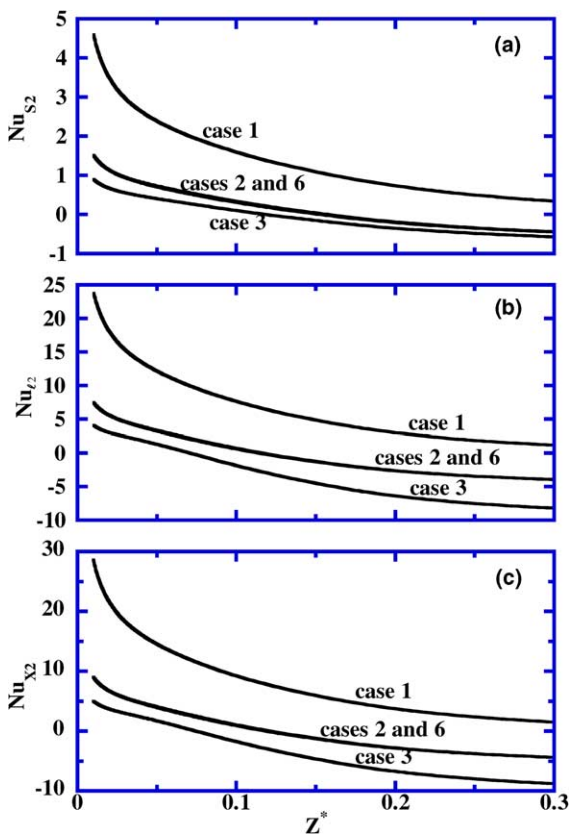

Fig. 10. Effects of wetted wall temperature T_1 on local Nusselt number distributions on the wetted wall 2 for $\gamma = 1$: (a) sensible heat Nusselt number; (b) latent heat Nusselt number; (c) interfacial Nusselt number.

increases. This is due to the larger combined buoyancy forces (i.e., Gr_T/Re and Gr_M/Re) for a system with a higher T_1. In Fig. 11(b), the negative Sherwood number along the wetted wall 2 indicates the existence of the condensation of water vapor on the wetted wall 2. Additionally, the Sherwood number decreases sharply for a larger T_1. This is because that the flow concentration of water vapor is higher than that on the wetted wall 2, resulting in the water vapor condensation on the wetted wall 2.

4.3. Effects of inlet relative humidity

It is interesting to examine the effect of the relative humidity of moist air at the inlet on the transport of latent heat exchange. Fig. 12 presents the effects of the relative humidity of moist air on the local latent heat Nusselt number along both wetted walls. In Fig. 12, a higher inlet relative humidity results in a lower latent heat Nusselt number in the same axial location for both wetted walls. It is also noted that the onset point of condensation is closer to the entrance for the case with more humid air mixture. As seen in Table 1, a lower relative humidity corresponds to a higher Gr_M. Heat transfer is strongly affected by species diffusion. This is because the species diffusion mechanism is more effective at lower concentration levels. This obviously indicates that the vaporization of the liquid film is reduced as the relative humidity increase.

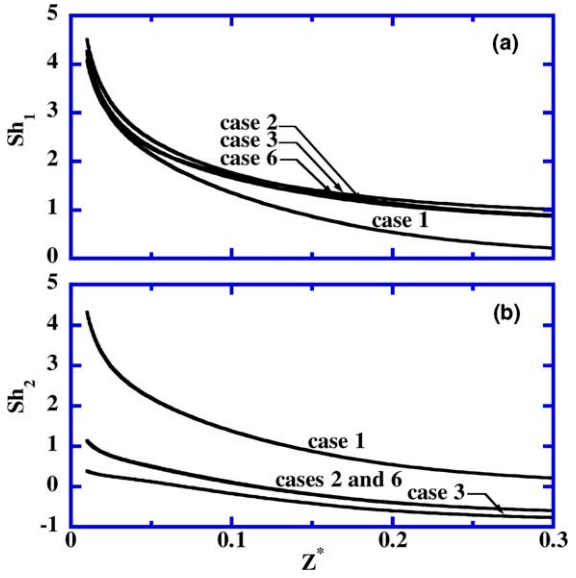

Fig. 11. Effects of wetted wall temperature T_1 on local Sherwood number distributions for $\gamma = 1$ on the (a) wetted wall 1 and (b) wetted wall 2.

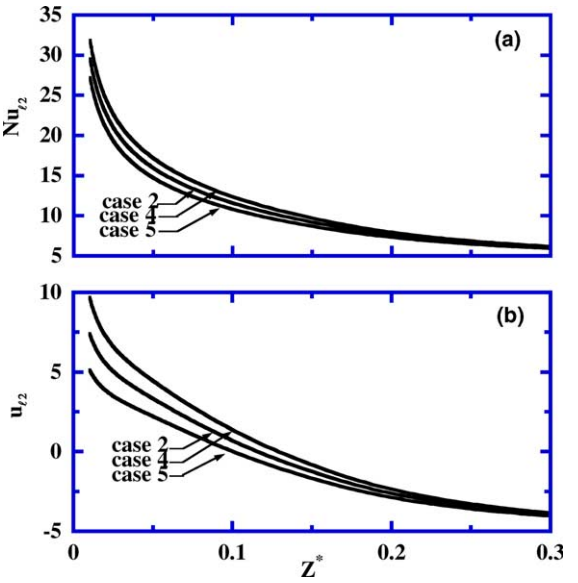

Fig. 12. Effects of relative humidity of moist air ϕ on latent heat Nusselt numbers for $\gamma = 1$ on the (a) wetted wall 1 and (b) wetted wall 2.

5. Conclusions

The problem of mixed convection heat and mass transfer in vertical rectangular ducts with film evaporation and condensation has been analyzed. The effects of aspect ratio γ of the duct, wetted wall temperature, Reynolds number of the flow and inlet relatively humidity on momentum, heat and mass transfer have been studied in detail. Brief summaries of the major results are listed in the following:

1. Film evaporation and condensation could take place on wetted wall 2. The temperature of moist air is lower than that of wetted wall 2 at the entrance region, film evaporation takes place. The temperature of moist air along the duct is increased and higher than the temperature of wetted wall 2, film condensation occurs.
2. A higher T_1 results in increasing friction coefficients, heat and mass transfer rates on wetted wall 1, and causing more water film condensation on wetted wall 2 due to a higher temperature of moist air.
3. Larger heat and mass transfer are noted with a greater γ. This is due to the wider porous wetted wall has a larger γ, which in turn, causes a greater film evaporation and condensation.
4. An increase in the relative humidity results in a decrease in heat transfer on both wetted walls 2. This is because the species diffusion mechanism is more effective at lower concentration levels.

Acknowledgments

The authors would like to acknowledge the financial support of the present work by the National Science Council, ROC through the contract NSC90-2212-E211-008. The financial support from Kuang-Wu Institute of Technology through project KW-91-ME-B01 is also acknowledged.

References

[1] W.J. Minkowycz, E.M. Sparrow, Condensation heat transfer in the presence of noncondensables, interfacial resistance, superheating, variable properties, and diffusion, Int. J. Heat Mass Transfer 9 (1966) 1125–1144.
[2] L. Wenzel, R.R. White, Drying granular solids in superheated steam, Ind. Engng. Chem. 43 (1951) 1829–1851.
[3] J.C. Chu, A.M. Lane, D. Conklin, Evaporation of liquids into their superheated vapour, Ind. Engng. Chem. 45 (1953) 1586–1591.
[4] L.C. Chow, J.N. Chung, Evaporation of water into a laminar stream of air and superheated steam, Int. J. Heat Mass Transfer 26 (3) (1983) 373–380.
[5] L.C. Chow, J.N. Chung, Water evaporation into a turbulent stream of air, humid air or superheated steam, in: Twenty-first ASME/AIChE National Heat Transfer Conference, Seattle, WA, ASME Paper No. 83-HT-2, 1983.
[6] C. Debbissi, J. Orfi, S. Ben Nasrallah, Evaporation of water by free convection in a vertical channel including effects of wall radiative properties, Int. J. Heat Mass Transfer 44 (2001) 811–826.
[7] C. Debbissi, J. Orfi, S. Ben Nasrallah, Evaporation of water by free or mixed convection into humid air and superheated steam, Int. J. Heat Mass Transfer 46 (2003) 4703–4715.
[8] Z.A. Hammou, B. Benhamou, N. Galanis, J. Orfi, Laminar mixed convection of humid air in a vertical channel with evaporation or condensation at the wall, Int. J. Thermal Sci. 43 (2004) 531–539.
[9] T.F. Lin, C.J. Chang, W.M. Yan, Analysis of combined buoyancy effects of thermal and mass diffusion on laminar forced convection heat transfer in a vertical tube, ASME J. Heat Transfer 110 (1988) 337–344.
[10] W.M. Yan, Y.L. Tsay, T.F. Lin, Simultaneous heat and mass transfer in laminar mixed convection flows between vertical parallel plates with asymmetric heating, Int. J. Heat Fluid Flow 10 (1989) 262–269.
[11] W.M. Yan, T.F. Lin, Effects of wetted wall on laminar mixed convection heat transfer in a vertical channel, J. Thermophys. Heat Transfer 3 (1989) 94–96.
[12] W.M. Yan, Mixed convection heat transfer enhancement through latent heat transport in vertical parallel plate channel flows, Can J. Chem. Engng. 69 (1991) 1277–1282.
[13] W.M. Yan, Turbulent mixed convection heat and mass transfer in a wetted channel, ASME J. Heat Transfer 117 (1995) 229–233.
[14] A.G. Fedorov, R. Viskanta, A.A. Mohamad, Turbulent heat and mass transfer in an asymmetrically heated, vertical parallel-plate channel, Int. J. Heat Fluid Flow 18 (1997) 307–315.
[15] J.N. Lin, P.Y. Tzeng, F.C. Chow, W.M. Yan, Convective instability of heat and mass transfer for laminar forced convection in the thermal entrance region of horizontal rectangular channels, Int. J. Heat Fluid Flow 13 (1992) 250–258.
[16] G.L. Hubbard, V.E. Denny, A.F. Mills, Droplet evaporation: effects of transients and variable properties, Int. J. Heat Mass Transfer 18 (1975) 1003–1008.
[17] T. Fujji, Y. Kato, K. Mihara, Expression of transport and thermodynamic properties of air, steam and water, Report No. 66, Department of Production Science, Kyushu University, Kyushu, Japan, 1977.
[18] R.B. Bird, W.E. Stewart, E.N. Lightfood, Transport Phenomena, Wily, New York, 1960.
[19] R.C. Reid, J.M. Prausnitz, T.K. Sherwood, The Properties of Gas and Liquid, Hemisphere/McGraw-Hill, New York, 1977 (Chapter 11).
[20] K. Ramakrishna, S.G. Rubin, P.K. Khosla, Laminar natural convection along vertical square ducts, Numer. Heat Transfer 5 (1982) 59–79.
[21] W.M. Yan, T.F. Lin, Combined heat and mass transfer in natural convection between vertical parallel plates with film evaporation, Int. J. Heat Mass Transfer 33 (1989) 529–541.
[22] F.P. Incropera, J.A. Schutt, Numerical simulation of laminar mixed convection in the entrance region of horizontal rectangular ducts, Numer. Heat Transfer 8 (1985) 707–729.
[23] H.V. Mahaney, F.P. Incropera, S. Ramadhyani, Development of laminar mixed convection flow in a horizontal rectangular duct with uniform bottom heating, Numer. Heat Transfer 12 (1987) 137–155.
[24] F.C. Chou, G.J. Hwang, Vorticity–velocity method for Graetz problem with effect of natural convection in a horizontal rectangular channel with uniform wall heat flux, J. Heat Transfer 109 (1987) 704–710.
[25] R.K. Shah, A.L. London, Laminar Flow Forced Convection in Duct, Academic Press, New York, 1978.
[26] S.V. Patankar, D.B. Spalding, A calculation procedure for heat, mass and momentum transfer in three-dimensional parabolic flows, Int. J. Heat Mass Transfer 15 (1972) 1784–1806.
[27] L.C. Burmeister, Convective Heat Transfer, McGraw-Hill, New York, 1983, pp. 170–174.
[28] W.M. Yan, H.Y. Li, Radiation effects on laminar mixed convection in an inclined square duct, ASME J. Heat Transfer 121 (1999) 194–200.
[29] M.M.M. Abou-Ellail, S.M. Morcos, Buoyancy effects in the entrance region of horizontal rectangular channels, Int. J. Heat Mass Transfer 105 (1983) 924–928.